

# Lsm12 Mediates Deubiquitination of DNA Polymerase $\eta$ To Help *Saccharomyces cerevisiae* Resist Oxidative Stress

Rui Yao,<sup>a,b,c</sup> Liujia Shi,<sup>a</sup> Chengjin Wu,<sup>b,c</sup> Weihua Qiao,<sup>b,c</sup> Liming Liu,<sup>b,c</sup> Jing Wu<sup>a</sup>

<sup>a</sup>School of Pharmaceutical Science, Jiangnan University, Wuxi, Jiangsu, China

<sup>b</sup>The Key Laboratory of Industrial Biotechnology, Ministry of Education, Jiangnan University, Wuxi, Jiangsu, China

<sup>c</sup>Laboratory of Food Microbial-Manufacturing Engineering, Jiangnan University, Wuxi, Jiangsu, China

**ABSTRACT** In *Saccharomyces cerevisiae*, the Y family DNA polymerase  $\eta$  (Pol $\eta$ ) regulates genome stability in response to different forms of environmental stress by translesion DNA synthesis. To elucidate the role of Pol $\eta$  in oxidative stress-induced DNA damage, we deleted or overexpressed the corresponding gene *RAD30* and used transcriptome analysis to screen the potential genes associated with *RAD30* to respond to DNA damage. Under 2 mM H<sub>2</sub>O<sub>2</sub> treatment, the deletion of *RAD30* resulted in a 2.2-fold decrease in survival and a 2.8-fold increase in DNA damage, whereas overexpression of *RAD30* increased survival and decreased DNA damage by 1.2- and 1.4-fold, respectively, compared with the wild-type strain. Transcriptome and phenotypic analyses identified Lsm12 as a main factor involved in oxidative stress-induced DNA damage. Deleting *LSM12* caused growth defects, while its overexpression enhanced cell growth under 2 mM H<sub>2</sub>O<sub>2</sub> treatment. This effect was due to the physical interaction of Lsm12 with the UBZ domain of Pol $\eta$  to enhance Pol $\eta$  deubiquitination through Ubp3 and consequently promote Pol $\eta$  recruitment. Overall, these findings demonstrate that Lsm12 is a novel regulator mediating Pol $\eta$  deubiquitination to promote its recruitment under oxidative stress. Furthermore, this study provides a potential strategy to maintain the genome stability of industrial strains during fermentation.

**IMPORTANCE** Pol $\eta$  was shown to be critical for cell growth in the yeast *Saccharomyces cerevisiae*, and deletion of its corresponding gene *RAD30* caused a severe growth defect under exposure to oxidative stress with 2 mM H<sub>2</sub>O<sub>2</sub>. Furthermore, we found that Lsm12 physically interacts with Pol $\eta$  and promotes Pol $\eta$  deubiquitination and recruitment. Overall, these findings indicate Lsm12 is a novel regulator mediating Pol $\eta$  deubiquitination that regulates its recruitment in response to DNA damage induced by oxidative stress.

**KEYWORDS** DNA damage, deubiquitination, oxidative stress, Pol $\eta$ , recruitment

Industrial microbial fermentation has been widely used in the production of chemicals. However, fermentation imposes a number of stresses on microorganisms, including oxidative stress, heat shock, osmotic stress, and exposure to toxic molecules and by-products (1–3). Most of these factors form reactive oxygen species (ROS) that can cause DNA damage and genome instability, resulting in cell cycle arrest and cell death, thereby decreasing synthesis of the target compound (4, 5). To solve this problem, cells have evolved a series of mechanisms for DNA damage tolerance.

In *Escherichia coli*, besides DNA repair mechanisms, such as base excision repair and mismatch repair, there are two major pathways to deal with DNA damage, homology-directed gap repair and translesion synthesis (TLS) (6). In the budding yeast *Saccharomyces cerevisiae*, there are three major strategies to maintain genome stability, template switch (TS) (7), homologous recombination (HR) (8), and TLS (9). TS is an error-free

**Citation** Yao R, Shi L, Wu C, Qiao W, Liu L, Wu J. 2019. Lsm12 mediates deubiquitination of DNA polymerase  $\eta$  to help *Saccharomyces cerevisiae* resist oxidative stress. *Appl Environ Microbiol* 85:e01988-18. <https://doi.org/10.1128/AEM.01988-18>.

**Editor** Shuang-Jiang Liu, Chinese Academy of Sciences

**Copyright** © 2018 American Society for Microbiology. All Rights Reserved.

Address correspondence to Jing Wu, wujing@jiangnan.edu.cn.

**Received** 13 August 2018

**Accepted** 13 October 2018

**Accepted manuscript posted online** 26 October 2018

**Published** 13 December 2018

damage branch of the DNA damage tolerance mechanism, which is regulated by the polyubiquitination of proliferating cell nuclear antigen (PCNA) catalyzed by the Ubc13 and Mms2 enzymes (7, 10, 11). HR mainly repairs DNA double-strand breaks and is regulated by Srs2 and Rad51 (11). Srs2 is a DNA helicase that can bind with *SIZ1*-mediated sumoylated PCNA to prevent HR, and Rad51 is a recombinase that promotes HR (12). Similar to TS, HR also belongs to the error-free branch of the DNA damage tolerance pathway (13). In contrast, TLS is referred to as the error-prone branch of DNA damage tolerance (14) and is a conserved mechanism from bacteria to mammals that recruits various specialized DNA polymerases to the stalled replication forks (15–17). These specialized polymerases mostly belong to the Y family, consisting of polymerase  $\eta$  (Pol $\eta$ ) and Rev1 in yeasts, encoded by *RAD30* and *REV1*, respectively (18). The B family polymerase  $\xi$  (Pol $\xi$ ) is also involved in TLS (19).

Pol $\eta$  was first identified in yeast and has been shown to play a dominant role in DNA damage tolerance. Previous studies also demonstrated that Pol $\eta$  was particularly efficient at bypassing UV radiation-induced cyclobutane pyrimidine dimers and could accurately insert an A opposite of the T of the dimer (20). Humans that lack Pol $\eta$  suffer from xeroderma pigmentosum variant, resulting in an extreme sensitivity to UV radiation (21). Pol $\eta$  can replicate 8-oxoguanine lesions efficiently and accurately by inserting a C opposite of the damage site (22). Pol $\eta$  can also bypass other lesions, such as (6-4)TT photoproducts (23), *O*-6-methylguanine (24), abasic sites (25), and DNA double-strand breaks (26). In *S. cerevisiae*, Pol $\eta$  is recruited to stalled replication forks by its physical interaction with monoubiquitinated PCNA (27). However, the precise mechanism by which Pol $\eta$  is recruited to PCNA and its specific role in the response to oxidative stress-induced DNA damage are unclear. Therefore, in this study, we evaluated the role of Pol $\eta$  in H<sub>2</sub>O<sub>2</sub>-induced oxidative stress and analyzed the underlying mechanism.

## RESULTS

***RAD30* is required for *S. cerevisiae* growth in the presence of H<sub>2</sub>O<sub>2</sub>.** First, we checked whether *RAD30* is required for the growth of *S. cerevisiae* in the presence of H<sub>2</sub>O<sub>2</sub>. Toward this end, the wild-type, *rad30* $\Delta$ , and *rad30* $\Delta$ /*RAD30* strains were spotted and grown on yeast nitrogen base medium with and without 2 mM H<sub>2</sub>O<sub>2</sub> exposure as a model of oxidative stress. The deletion of *RAD30* caused a significant growth defect in the presence of 2 mM H<sub>2</sub>O<sub>2</sub>, whereas overexpression of *RAD30* enhanced growth compared to that of the wild-type strain (Fig. 1A). Survival curves for all three strains were determined over a broad concentration range of H<sub>2</sub>O<sub>2</sub> (Fig. 1B). At 2 mM H<sub>2</sub>O<sub>2</sub> exposure, 70.4% of the wild-type strain survived, while the *rad30* $\Delta$  mutant and *rad30* $\Delta$ /*RAD30* strains exhibited reduced (31.7%) and increased (84.5%) survival, representing a 2.2-fold decrease and 1.2-fold increase, respectively. These results suggest that *RAD30* contributes to cell growth in the presence of H<sub>2</sub>O<sub>2</sub>.

To investigate the underlying mechanism, single-cell gel electrophoresis of the wild-type, *rad30* $\Delta$  mutant, and *rad30* $\Delta$ /*RAD30* strains was performed. Without H<sub>2</sub>O<sub>2</sub> treatment, both the *rad30* $\Delta$  mutant and *rad30* $\Delta$ /*RAD30* strains displayed similar tail lengths relative to the wild-type strain. However, when treated with 2 mM H<sub>2</sub>O<sub>2</sub>, the *rad30* $\Delta$  mutant and *rad30* $\Delta$ /*RAD30* strains showed a 2.8-fold increase and 1.4-fold decrease in tail length, respectively, compared to that of the wild-type strain (Fig. 1C). This suggests that *RAD30* may play an important role in the response of *S. cerevisiae* to H<sub>2</sub>O<sub>2</sub>-induced DNA damage.

**Global transcriptome analysis of the *rad30* $\Delta$  and wild-type strains after treatment with H<sub>2</sub>O<sub>2</sub>.** To further explain the weaker growth of the *rad30* $\Delta$  strain in the presence of H<sub>2</sub>O<sub>2</sub>, transcriptome sequencing was conducted to compare gene expression profiles in the *rad30* $\Delta$  mutant and wild-type strains. Restrictive thresholds [ $|\log_2(\text{fold change})| \geq 1$ ; false-discovery rate (FDR),  $<0.05$ ] of differentially expressed (DE) genes were used to screen the genes. First, we analyzed the DE genes under H<sub>2</sub>O<sub>2</sub> treatment conditions relative to the normal condition in both wild-type and *rad30* $\Delta$  mutant strains (Fig. 2A). Transcriptional profiling and Gene Ontology (GO) term enrich-

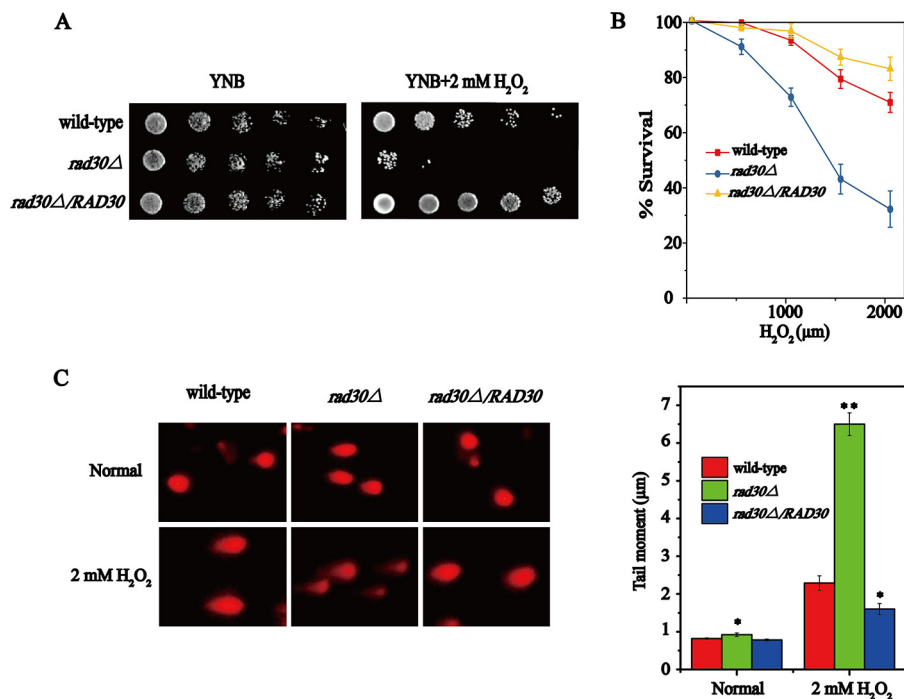


**FIG 1** *RAD30* is required for *S. cerevisiae* growth in the presence of H<sub>2</sub>O<sub>2</sub>. (A) Wild-type, *rad30Δ* mutant, and *rad30Δ/RAD30* strains were spotted on YNB plates under normal and 2 mM H<sub>2</sub>O<sub>2</sub> treatment conditions. (B) The survival rates of wild-type, *rad30Δ* mutant, and *rad30Δ/RAD30* cells over a range of H<sub>2</sub>O<sub>2</sub> doses (0, 500, 1,000, 1,500, and 2,000 μM). (C) Comet assay in wild-type, *rad30Δ* mutant, and *rad30Δ/RAD30* strains exposed to normal or 2 mM H<sub>2</sub>O<sub>2</sub> conditions. Data represent the means of three biological replicates ( $n = 3$ ), and error bars represent the standard deviation. \*,  $P \leq 0.05$ ; \*\*,  $P \leq 0.01$ .

ment analysis revealed that carbohydrate metabolism and amino acid metabolism were the most affected pathways in the wild-type strain; the same results were obtained in the *rad30Δ* mutant strain. Additionally, 64 DE genes were common between wild-type and *rad30Δ* mutant strains and consisted of 49 upregulated and 15 downregulated genes; all the genes are listed in Table S1 in the supplemental material. The commonly upregulated genes were involved in the DNA recombination process, DNA damage response, zinc ion homeostasis, and oxidative stress response, whereas the commonly downregulated genes were enriched in GO processes, such as cell wall chitin metabolism, the mitotic cell cycle, and transport.

Next, the DE genes in the *rad30Δ* mutant relative to those in the wild type were analyzed under both normal and H<sub>2</sub>O<sub>2</sub> treatment conditions (Fig. 2B). Under normal conditions, DE genes were involved in amino acid metabolism and RNA metabolism; however, under 2 mM H<sub>2</sub>O<sub>2</sub> treatment, the DE genes were involved in DNA replication and cellular response to stress. Between the two conditions, there was a total of 68 common DE genes, consisting of 27 upregulated and 41 downregulated genes (Table S2). GO analysis showed that the commonly upregulated genes were involved in amino acid metabolism, protein folding, and DNA binding, whereas the commonly downregulated genes were enriched in processes, such as meiosis I, adenine metabolism, DNA damage response, and RNA metabolism.

Among the genes commonly downregulated in the *rad30Δ* mutant strain, *VHR2*, *BAP3*, *PHO3*, *LSM12*, *YHB1*, *PTR2*, *CAR1*, and *NDE1* were the most significantly altered between the strains, with 3.36-, 3.42-, 2.84-, 2.56-, 2.22-, 2.49-, 2.77-, and 3.05-fold differences, respectively, under the normal conditions, and with 2.2-, 2.63-, 2.79-, 2.41-, 1.85-, 2.55-, 2.09-, and 1.55-fold differences, respectively, under 2 mM H<sub>2</sub>O<sub>2</sub> treatment. These results were further verified by reverse transcription-PCR (RT-PCR) analysis (Fig. 2C and D). To test whether these proteins interact with Pol $\eta$  or act in the same pathway, these genes were deleted or overexpressed in each strain, and the conse-

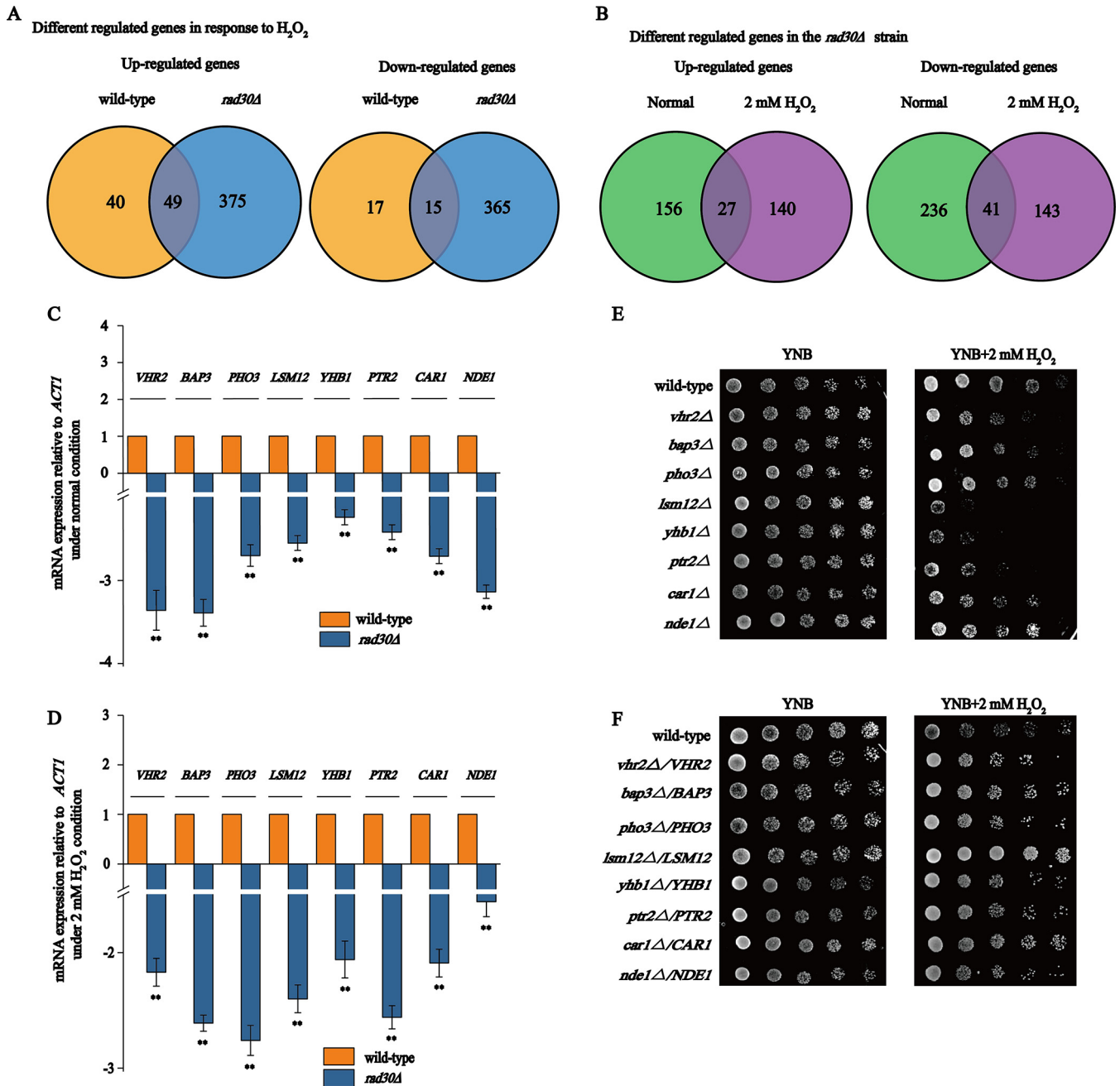


**FIG 2** *LSM12* is involved in DNA damage tolerance. (A) Venn diagrams depicting the numbers of upregulated and downregulated genes in wild-type and *rad30Δ* mutant strains under normal conditions compared with the gene expression levels in the corresponding strains under the 2 mM H<sub>2</sub>O<sub>2</sub> treatment conditions. (B) Numbers of upregulated and downregulated genes in the *rad30Δ* mutant relative to their expression in the wild-type strain under normal and 2 mM H<sub>2</sub>O<sub>2</sub> treatment conditions. (C and D) Quantitative reverse transcription-PCR (qRT-PCR) verified the mRNA expression levels of the most commonly downregulated genes, calculated relative to the *ACT1* level, under normal and 2 mM H<sub>2</sub>O<sub>2</sub> treatment conditions. Data represent the means of three biological replicates (*n* = 3), and error bars represent the standard deviation. \*\*, *P* ≤ 0.01. (E) The most commonly downregulated genes were deleted, and the mutant strains were spotted on YNB plates under normal and 2 mM H<sub>2</sub>O<sub>2</sub> treatment conditions. (F) The most commonly downregulated genes were overexpressed, and the mutant strains were spotted on YNB plates under normal and 2 mM H<sub>2</sub>O<sub>2</sub> treatment conditions.

quence on resistance to H<sub>2</sub>O<sub>2</sub> stress was evaluated. Interestingly, the deletion of *VHR2*, *LSM12*, or *YHB1* caused growth defects under 2 mM H<sub>2</sub>O<sub>2</sub> treatment conditions (Fig. 2E); however, only overexpression of *LSM12* conferred resistance to H<sub>2</sub>O<sub>2</sub> (Fig. 2F). Based on these results, we hypothesized that *LSM12* may coordinate with *RAD30* to play an important role in DNA damage tolerance.

**Polη interacts with Lsm12 through the UBZ domain.** On the basis of the above-mentioned results, the subcellular localization of Polη and Lsm12 was de-

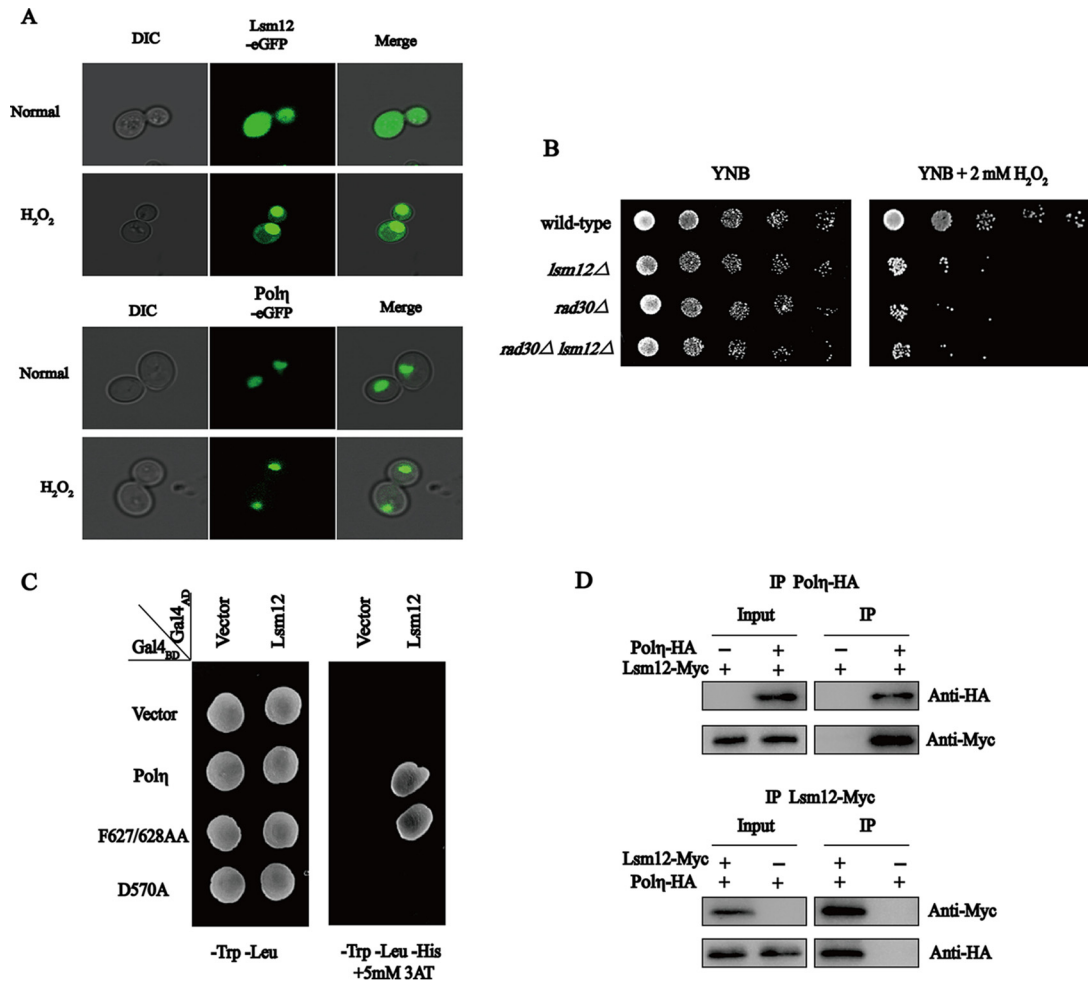


**FIG 3** Pol $\eta$  interacts with Lsm12 through the UBZ domain. (A) Pol $\eta$  and Lsm12 were fused with the eGFP reporter and overexpressed, and the subcellular localization was visualized under normal and 2 mM H<sub>2</sub>O<sub>2</sub> treatment conditions. (B) The wild-type and *lsm12*Δ, *rad30*Δ, and *rad30*Δ *lsm12*Δ mutant strains were spotted on YNB plates with or without H<sub>2</sub>O<sub>2</sub>. (C) Yeast two-hybrid assays confirmed the interaction between Pol $\eta$  and Lsm12; the D570A mutant failed to interact with Lsm12. (D) Coimmunoprecipitation assay to detect the interaction between Pol $\eta$  and Lsm12 *in vivo*. IP, immunoprecipitation.

terminated. Under the normal conditions, Lsm12 localized both in the nucleus and cytoplasm; however, following treatment with 2 mM H<sub>2</sub>O<sub>2</sub>, Lsm12 was mostly detected in the nucleus (Fig. 3A). In contrast, Pol $\eta$  was located in the nucleus both with and without H<sub>2</sub>O<sub>2</sub> treatment. These results indicated that the relative distribution of Lsm12 in the nucleus increased with H<sub>2</sub>O<sub>2</sub> treatment, supporting the hypothesis that Pol $\eta$  and Lsm12 may function together in the response to H<sub>2</sub>O<sub>2</sub> treatment in the nucleus.

To further confirm this mechanism, we next examined the direct relationship between Lsm12 and Pol $\eta$ . First, the genetic interaction between Lsm12 and Pol $\eta$  was evaluated using spot assays, which revealed that the phenotype of the *rad30*Δ *lsm12*Δ double mutant was similar to those of the *rad30*Δ and *lsm12*Δ single mutants (Fig. 3B). Moreover, the *rad30*Δ *lsm12*Δ double mutant showed 33.6% survival, whereas the *rad30*Δ and *lsm12*Δ single mutants exhibited 31.7% and 36.5% survival, respectively (Table 1). These results demonstrated that the two genes have epistatic interactions.

Next, the physical interaction between Lsm12 and Pol $\eta$  was determined. As shown in Fig. 3C, the yeast two-hybrid (Y2H) analysis revealed a gene-specific interaction between the full-length Lsm12 and Pol $\eta$ . To further identify the regions within Pol $\eta$  responsible for its interaction with Lsm12, the FF627/628AA and D570A mutant strains were constructed, in which the PIP (PCNA-interacting protein) and

**TABLE 1** H<sub>2</sub>O<sub>2</sub> sensitivity of various yeast strains

Strain	Survival <sup>a</sup> (SD) (%)	
	Without H <sub>2</sub> O <sub>2</sub>	2 mM H <sub>2</sub> O <sub>2</sub> treatment
Wild type	100	70.4 (3.9)
<i>rad30Δ</i> mutant	99.8 (1.64)	31.7 (4.9) <sup>b</sup>
<i>rad30Δ/RAD30</i> strain	98.1 (1.48)	84.5 (4.1) <sup>b</sup>
<i>lsm12Δ</i> mutant	98.5 (2.26)	36.5 (4.7) <sup>b</sup>
<i>rad30Δ lsm12Δ</i> mutant	96.3 (0.75)	33.6 (2.2) <sup>b</sup>
<i>ubp3Δ</i> mutant	98.1 (1.74)	40.7 (3.6) <sup>b</sup>
<i>lsm12Δ ubp3Δ</i> mutant	96.1 (2.22)	34.3 (1.9) <sup>b</sup>

<sup>a</sup>Survival rates, with the standard deviations shown, are expressed relative to those of wild-type cells. Results are the averages from three experiments.

<sup>b</sup>*P* values versus WT of  $\leq 0.01$ .

UBZ (ubiquitin-binding zinc finger) domains, respectively, were inactivated. The PIP domain is known to interact with monoubiquitylated PCNA and to be important in DNA damage tolerance (28), and the UBZ domain has also been reported to be involved in DNA damage tolerance. Recent studies showed that the UBZ domain could interact with some proteins to contribute to the DNA damage response (29). In our results, the FF627/628AA mutant, but not the D570A mutant, also interacted with Lsm12 (Fig. 3C). Furthermore, coimmunoprecipitation assays confirmed that Lsm12 and Pol $\eta$  physically interact *in vivo* (Fig. 3D), whereas this interaction did not occur with the D570A mutant, consistent with the Y2H results (data not shown). These observations suggest that Lsm12 physical interacts with Pol $\eta$  at the UBZ domain.

**Lsm12 promotes Pol $\eta$  recruitment in the presence of H<sub>2</sub>O<sub>2</sub>.** Given the genetic and physical interaction between Lsm12 and Pol $\eta$ , we supposed that Lsm12 likely plays a role in DNA damage tolerance. Therefore, we next explored the mechanism by which Lsm12 repairs or facilitates tolerance to H<sub>2</sub>O<sub>2</sub>-induced DNA damage. The deletion of *LSM12* did not affect the mRNA or protein levels of Pol $\eta$  compared with those of the wild type (data not shown). However, under H<sub>2</sub>O<sub>2</sub> treatment, the deletion of *LSM12* led to a decrease in the number of Pol $\eta$  foci formed, at only 37.2%, in contrast to the 69.5% foci detected in the wild-type strain (Fig. 4A and B). To further examine this result, the number of foci in the two strains after treatment with methyl methanesulfonate (MMS) were measured. Similarly, there were 76.2% and 43.3% Pol $\eta$  foci in the wild-type and *lsm12Δ* mutant strains, respectively. These results suggest that Lsm12 promotes Pol $\eta$  recruitment to facilitate tolerance of DNA damage.

**Lsm12 deubiquitinates Pol $\eta$  through Ubp3.** To elucidate the mechanism underlying the effect of Lsm12 in enhancing the formation of Pol $\eta$  foci in *S. cerevisiae*, the levels of PCNA and Pol $\eta$  monoubiquitination were compared in the wild-type and *lsm12Δ* mutant strains without and with H<sub>2</sub>O<sub>2</sub> treatment. As shown in Fig. 5A and B, the

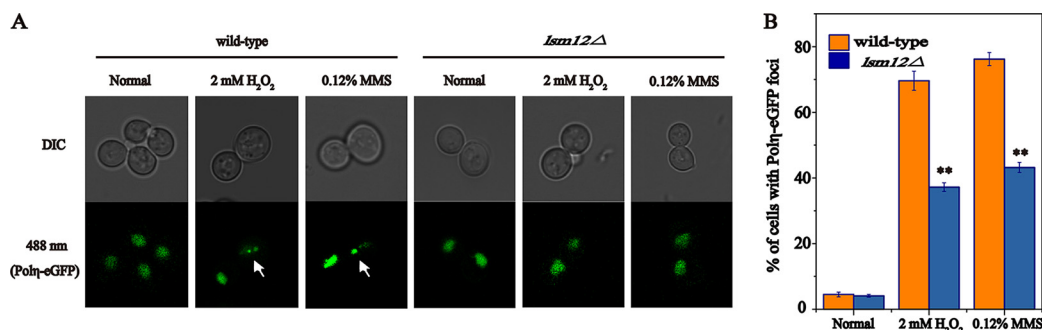


**FIG 4** Lsm12 promotes Pol $\eta$  focus formation. (A) Formation of Pol $\eta$  foci when cells of wild-type and *lsm12Δ* mutant strains were treated with different DNA-damaging agents. (B) Percentage of cells of different strains displaying Pol $\eta$ -eGFP foci in different environments. The histograms represent the mean  $\pm$  standard deviation from three independent experiments. \*\*, *P*  $\leq 0.01$ .

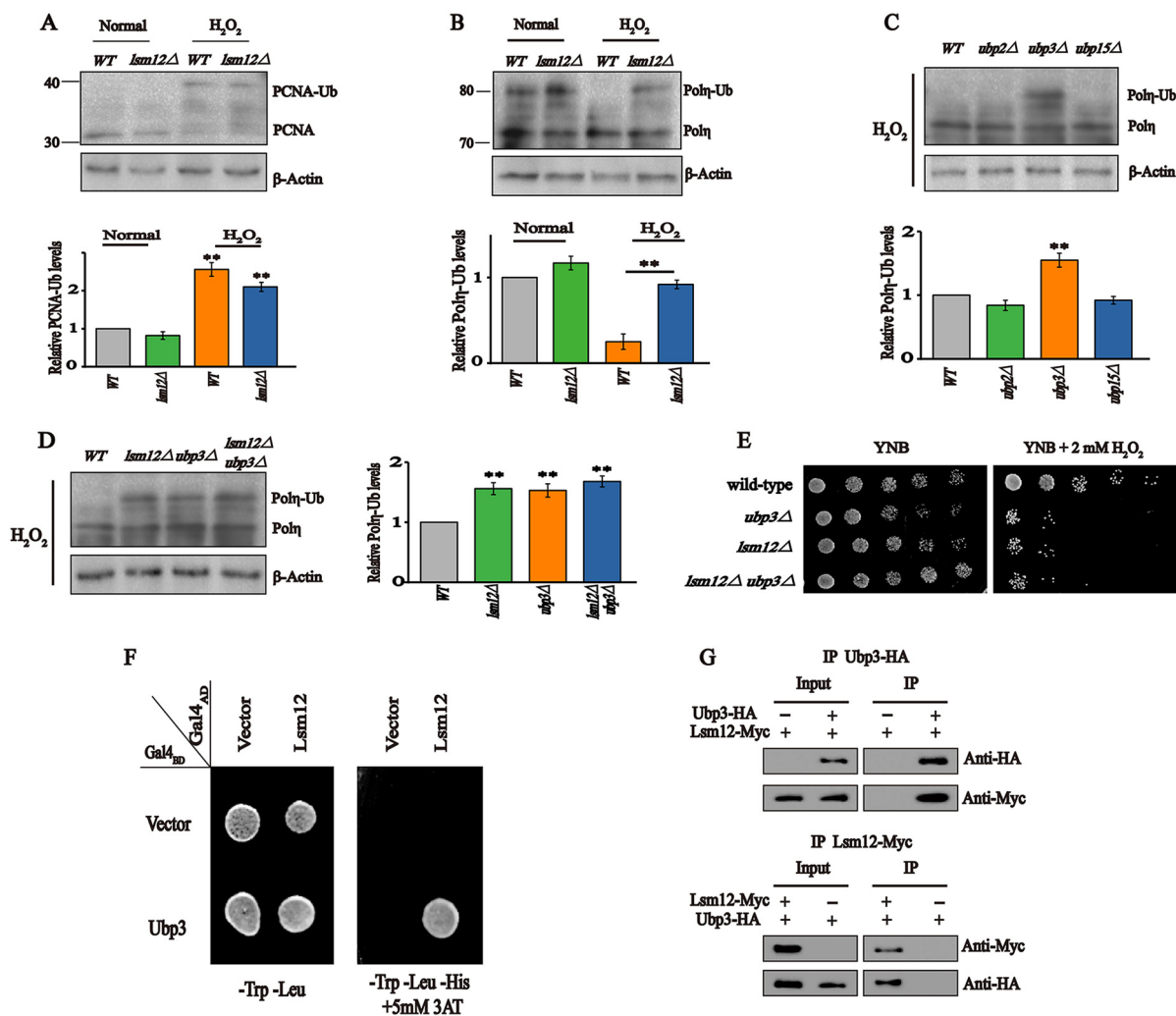


**FIG 5** Lsm12 promoted Pol $\eta$  deubiquitination through Ubp3. (A) The level of monoubiquitinated PCNA in the wild-type and *lsm12* $\Delta$  mutant strains. (B to D) The level of monoubiquitinated Pol $\eta$  in the wild-type strain and *lsm12* mutant (B), *ubp2* $\Delta$ , *ubp3* $\Delta$ , and *ubp15* $\Delta$  mutant (C), and *ubp3* $\Delta$ , *lsm12* $\Delta$ , and *ubp3* $\Delta$  *lsm12* $\Delta$  mutant (D) strains.  $\beta$ -Actin was used as a loading control. Data represent means of three biological replicates ( $n = 3$ ), and error bars represent the standard deviation. \*\*,  $P \leq 0.01$ . (E) Spot assays in the wild-type and *ubp3* $\Delta$ , *lsm12* $\Delta$ , and *ubp3* $\Delta$  *lsm12* $\Delta$  mutant strains with or without H<sub>2</sub>O<sub>2</sub>. (F) Yeast two-hybrid assays confirmed the interaction between Lsm12 and Ubp3. (G) Coimmunoprecipitation assay to detect the interaction between Lsm12 and Ubp3 *in vivo*.

level of PCNA monoubiquitination significantly increased in both the wild-type (120%) and *lsm12* $\Delta$  mutant (94%) strains after 2 mM H<sub>2</sub>O<sub>2</sub> treatment, and there was no difference between the strains under either condition. In contrast, the level of Pol $\eta$  monoubiquitination significantly decreased in the wild type (42%) after 2 mM H<sub>2</sub>O<sub>2</sub> treatment and was 102% higher in the *lsm12* $\Delta$  mutant strain. This difference in the effects on PCNA and Pol $\eta$  monoubiquitination demonstrated that Lsm12 enhances Pol $\eta$  deubiquitination to promote Pol $\eta$  recruitment.

Given the lack of evidence that Lsm12 has its own deubiquitination activity, we hypothesized that Lsm12 binds with some deubiquitinase to catalyze the deubiquitination of Pol $\eta$ . To identify the specific deubiquitinase, we focused on the *UBP2*, *UBP3*, and *UBP15* genes, which are known to be associated with DNA damage tolerance. Under H<sub>2</sub>O<sub>2</sub> treatment, the deletion of *UBP2* and *UBP15* did not affect the level of Pol $\eta$  monoubiquitination compared with that of the wild type, whereas the deletion of *UBP3* increased Pol $\eta$  monoubiquitination (75%) (Fig. 5C). Moreover, the level of Pol $\eta$  monoubiquitination in the *lsm12* $\Delta$  *ubp3* $\Delta$  double mutant was similar to that of the *lsm12* $\Delta$  and *ubp3* $\Delta$  single mutants under H<sub>2</sub>O<sub>2</sub> treatment conditions (Fig. 5D). Spot and survival

assays also showed that the phenotype of the *lsm12Δ ubp3Δ* double mutant was similar to those of the two single mutants (Fig. 5E and Table 1). Further, both Y2H and coimmunoprecipitation experiments verified the physical interaction of Ubp3 with Lsm12 (Fig. 5F and G), and this interaction was strengthened by 16% when cells were treated with 2 mM H<sub>2</sub>O<sub>2</sub> (Fig. S1). These results suggest that Lsm12 promotes the deubiquitination of Pol $\eta$ , likely by binding with Ubp3.

## DISCUSSION

Translesion synthesis is a key pathway to maintain genome stability; however, the precise molecular mechanisms involved have not yet been clarified in detail. In this study, we demonstrated that the deletion of *RAD30* caused a severe growth defect in the yeast *S. cerevisiae*, while its overexpression enhanced growth under oxidative stress due to exposure to 2 mM H<sub>2</sub>O<sub>2</sub>. The stress response involves physical interaction between Lsm12 and Pol $\eta$  to tolerate or repair the consequent DNA damage. As a result, Lsm12 promoted Pol $\eta$  deubiquitination and facilitated Pol $\eta$  focus formation. These results demonstrate that Lsm12 mediates Pol $\eta$  deubiquitination and regulates its recruitment to help cells resist oxidative stress.

Previous studies have also indicated that *RAD30* appears to regulate cell growth under H<sub>2</sub>O<sub>2</sub>-induced DNA damage. In *S. cerevisiae*, cells lacking this gene are sensitive to UV radiation (30), MMS (31), and hydroxyurea (32). Yeast overexpressing Pol $\eta$  from *Trypanosoma cruzi* were reported to be more resistant to H<sub>2</sub>O<sub>2</sub> exposure than the wild type (33). In human cells, a loss of *POLH*, the orthologous gene to *RAD30* in *S. cerevisiae*, resulted in increased sensitivity to oxidative stress (34). Furthermore, knockdown of Pol $\eta$  in human cells decreased cell survival and accelerated DNA damage and apoptosis (28). In our study, the deletion of *RAD30* exhibited a severe growth defect, whereas overexpression of *RAD30* enhanced cell growth compared to that of the wild-type strain under 2 mM H<sub>2</sub>O<sub>2</sub> treatment. This phenomenon was consistent with the previous findings in human cells, suggesting that Pol $\eta$  is a highly conserved protein from yeast to humans.

Lsm12 seems to be a multifunctional protein. Indeed, a previous study demonstrated that Lsm12 was involved in many aspects of RNA processing, such as mRNA degradation, tRNA splicing, pre-mRNA splicing and degradation, and rRNA processing (35). In addition, Lee et al. (36) demonstrated that Lsm12 is involved in DNA replication stress. The present study provides new insight into this mechanism, showing that Lsm12 interacted with Pol $\eta$  to respond to the DNA damage induced by oxidative stress, and that this interaction occurs on the UBZ domain of Pol $\eta$ . In *S. cerevisiae*, Pol $\eta$  has two conserved domains, PIP and UBZ; the PIP domain includes the F627 and F628 residues, and the UBZ domain includes the D570 residue (18). The PIP domain mainly interacts with monoubiquitinated PCNA when DNA is damaged (28). However, the function of the UBZ domain is not fully understood. A recent study showed that an inactive UBZ domain (*RAD30-D570A* mutant) failed to complement the phenotype of the *rad30Δ* mutant (37). Moreover, the UBZ domain of Pol $\eta$  was shown to be essential for 8-oxoguanine-induced mutagenesis (38). Additionally, Lsm12-green fluorescent protein (Lsm12-GFP) accumulated in the nucleus when yeast cells were treated with 2 mM H<sub>2</sub>O<sub>2</sub> (Fig. 3A), vaguely implying that the physical interaction between Pol $\eta$  and Lsm12 was enhanced when cells were exposed to oxidative stress. Our results indicated that the physical interaction between Pol $\eta$  and Lsm12 was increased by 14% under the 2 mM H<sub>2</sub>O<sub>2</sub> conditions compared to the normal conditions (Fig. S2).

Here, we demonstrate that Lsm12 promoted Pol $\eta$  deubiquitination and recruitment. When cells are under DNA replication stress, the Y family of DNA polymerases is recruited to the stalled replication forks (39). In this study, the deletion of *LSM12* decreased the rate of Pol $\eta$  focus formation under H<sub>2</sub>O<sub>2</sub> treatment conditions, indicating that the absence of Lsm12 decreased Pol $\eta$  recruitment. This is likely due to two mechanisms, as follows: (i) increasing PCNA monoubiquitination might promote Pol $\eta$  recruitment, because PCNA monoubiquitination can enhance affinity with Y family DNA polymerases (40), and Rad6/Rad18 induced PCNA monoubiquitination is essential for Pol $\eta$  recruitment (41); and (ii) decreasing Pol $\eta$  monoubiquitination might promote Pol $\eta$



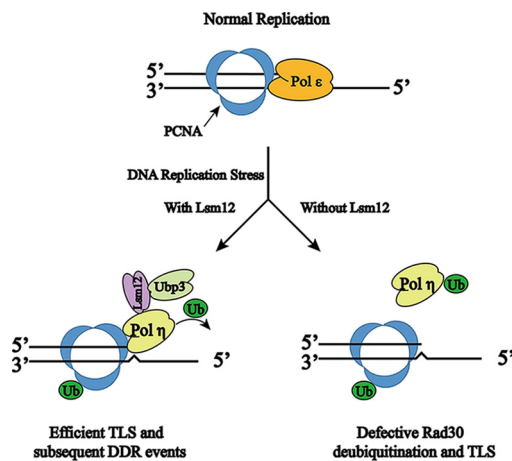


**FIG 6** Model depicting the molecular function of Lsm12. When cells are under DNA replication stress, Lsm12 binds with Ubp3 and promotes the deubiquitination of Pol $\eta$ , which activates the TLS pathway. In the absence of Lsm12, cells fail to deubiquitinate Pol $\eta$ , causing defective TLS. DDR, DNA damage response.

recruitment. Previous studies indicated that when cells were exposed to UV radiation, the level of Pol $\eta$  monoubiquitination was downregulated in the S-phase as a response to DNA damage (42). Similar results have also been detected in human cells (43). In this study, Lsm12 enhanced Pol $\eta$  recruitment through another mechanism, given the observed decrease in the level of Pol $\eta$  monoubiquitination. However, this raises the question as to how Lsm12 deubiquitinates Pol $\eta$ . In *S. cerevisiae*, three deubiquitinases may be responsible for Pol $\eta$  deubiquitination, Ubp15, Ubp2, and Ubp3. Ubp15 leads to the accumulation of the mono-, di-, and polyubiquitination forms of PCNA (44). Ubp2 has been associated with oxidative stress, and the homologous gene in humans was shown to play a role in DNA damage tolerance (44). Ubp3 also appears to be involved in DNA replication stress, given that a global protein abundance analysis revealed that the level of Ubp3 increased in response to exposure to DNA-damaging agents (45). Moreover, Ubp3 can stabilize Rad4 to enhance UV resistance and promote the repair of UV-induced DNA damage (46). In this study, only the *ubp3 $\Delta$  mutant was found to increase the Pol $\eta$  monoubiquitination level, and genetic analyses further showed that *UBP3* and *LSM12* were epistatic. Accordingly, these two genes may function together in the deubiquitination of Pol $\eta$ . Both the Y2H and coimmunoprecipitation experiments confirmed a physical interaction between Lsm12 and Ubp3, which further validated our hypothesis.*

In summary, we have identified a function of Lsm12 in the response to oxidative stress-induced DNA damage through interaction with Pol $\eta$  to promote Pol $\eta$  deubiquitination and recruitment. When cells were subjected to oxidative DNA replication stress, the amount of Lsm12 in the nucleus was increased, thereby promoting Pol $\eta$  deubiquitination and further facilitating Pol $\eta$  recruitment, to ultimately activate the TLS pathway and bypass DNA lesions. Cells with *LSM12* deleted failed to deubiquitinate Pol $\eta$ , leading to a defective TLS pathway (Fig. 6). These findings provide new insights into the molecular mechanisms of oxidative stress-induced DNA damage and suggest potential strategies to maintain the genomic stability of industrial strains.

## MATERIALS AND METHODS

**Yeast strains, plasmids, and growth conditions.** The *Saccharomyces cerevisiae* strains and plasmids used in this study are listed in Table 2. The deletion strains were constructed by homologous recombination (47), the *LEU2* or *HIS3* marker was fused to the upstream and downstream regions of the target gene open reading frame by fusion-PCR, and the PCR products were transformed into wild-type cells using the lithium acetate transformation method. For the overexpression strains, we used the GPD promoter of plasmid pY26; the target genes were amplified from the genome of *BY4741* using primers containing HindIII and XhoI restriction sites (for *RAD30*) and cloned into pY26 to generate pY26-*RAD30*, pY26-*VHR2*, pY26-*BAP3*, pY26-*PHO3*, pY26-*LSM12*, pY26-*YHB1*, pY26-*PTR2*, pY26-*CAR1*, and pY26-*NDE1*.

**TABLE 2** Strains and plasmids used in this study

Strain or plasmid	Relevant characteristic	Reference or source
<b>Strains</b>		
BY4741	<i>Mata his3Δ1 leu2Δ0 met15Δ0 ura3Δ0</i>	This study
<i>rad30Δ</i> mutant	<i>Mata his3Δ1 leu2Δ0 met15Δ0 ura3Δ0 RAD30::LEU2</i>	This study
<i>uhr2Δ</i> mutant	<i>Mata his3Δ1 leu2Δ0 met15Δ0 ura3Δ0 VHR2::HIS3</i>	This study
<i>bap3Δ</i> mutant	<i>Mata his3Δ1 leu2Δ0 met15Δ0 ura3Δ0 BAP3::HIS3</i>	This study
<i>pho3Δ</i> mutant	<i>Mata his3Δ1 leu2Δ0 met15Δ0 ura3Δ0 PHO3::HIS3</i>	This study
<i>lsm12Δ</i> mutant	<i>Mata his3Δ1 leu2Δ0 met15Δ0 ura3Δ0 LSM12::HIS3</i>	This study
<i>yhb1Δ</i> mutant	<i>Mata his3Δ1 leu2Δ0 met15Δ0 ura3Δ0 YHB1::HIS3</i>	This study
<i>ptr2Δ</i> mutant	<i>Mata his3Δ1 leu2Δ0 met15Δ0 ura3Δ0 PTR2::HIS3</i>	This study
<i>car1Δ</i> mutant	<i>Mata his3Δ1 leu2Δ0 met15Δ0 ura3Δ0 CAR1::HIS3</i>	This study
<i>nde1Δ</i> mutant	<i>Mata his3Δ1 leu2Δ0 met15Δ0 ura3Δ0 NDE1::HIS3</i>	This study
<i>ubp2Δ</i> mutant	<i>Mata his3Δ1 leu2Δ0 met15Δ0 ura3Δ0 UBP2::HIS3</i>	This study
<i>ubp3Δ</i> mutant	<i>Mata his3Δ1 leu2Δ0 met15Δ0 ura3Δ0 UBP3::HIS3</i>	This study
<i>ubp15Δ</i> mutant	<i>Mata his3Δ1 leu2Δ0 met15Δ0 ura3Δ0 UBP15::HIS3</i>	This study
<i>rad30Δ lsm12Δ</i> mutant	<i>Mata his3Δ1 leu2Δ0 met15Δ0 ura3Δ0 RAD30::LEU2 LSM12::HIS3</i>	This study
<i>rad30Δ ubp3Δ</i> mutant	<i>Mata his3Δ1 leu2Δ0 met15Δ0 ura3Δ0 RAD30::LEU2 UBP3::HIS3</i>	This study
<i>rad30Δ/RAD30</i> strain	<i>Mata his3Δ1 leu2Δ0 met15Δ0 ura3Δ0 RAD30::LEU2pY26- P<sub>GPD</sub>/RAD30</i>	This study
<i>uhr2Δ/VHR2</i> strain	<i>Mata his3Δ1 leu2Δ0 met15Δ0 ura3Δ0 VHR2::HIS3pY26- P<sub>GPD</sub>/VHR2</i>	This study
<i>bap3Δ/BAP3</i> strain	<i>Mata his3Δ1 leu2Δ0 met15Δ0 ura3Δ0 BAP3::HIS3pY26- P<sub>GPD</sub>/BAP3</i>	This study
<i>pho3Δ/PHO3</i> strain	<i>Mata his3Δ1 leu2Δ0 met15Δ0 ura3Δ0 PHO3::HIS3pY26- P<sub>GPD</sub>/PHO3</i>	This study
<i>lsm12Δ/LSM12</i> strain	<i>Mata his3Δ1 leu2Δ0 met15Δ0 ura3Δ0 LSM12::HIS3pY26- P<sub>GPD</sub>/LSM12</i>	This study
<i>yhb1Δ/YHB1</i> strain	<i>Mata his3Δ1 leu2Δ0 met15Δ0 ura3Δ0 YHB1::HIS3pY26- P<sub>GPD</sub>/YHB1</i>	This study
<i>ptr2Δ/PTR2</i> strain	<i>Mata his3Δ1 leu2Δ0 met15Δ0 ura3Δ0 PTR2::HIS3pY26- P<sub>GPD</sub>/PTR2</i>	This study
<i>car1Δ/CAR1</i> strain	<i>Mata his3Δ1 leu2Δ0 met15Δ0 ura3Δ0 CAR1::HIS3pY26- P<sub>GPD</sub>/CAR1</i>	This study
<i>nde1Δ/NDE1</i> strain	<i>Mata his3Δ1 leu2Δ0 met15Δ0 ura3Δ0 NDE1::HIS3pY26- P<sub>GPD</sub>/NDE1</i>	This study
AH109 mutant	<i>trp1Δ leu2 ura3Δ his3Δ gal4Δ gal80ΔLYS2::GAL1<sub>UAS</sub>-GAL1<sub>TATA</sub>-HIS3 GAL2<sub>UAS</sub>-GAL2<sub>TATA</sub>-ADE2 URA3::MEL1<sub>UAS</sub>-MEL1<sub>TATA</sub>-LacZ MEL1</i>	Clontech
BY4741 RAD30-HA LSM12-Myc mutant	<i>Mata his3Δ1 leu2Δ0 met15Δ0 ura3Δ0 RAD30::LEU2 LSM12::HIS3; pY26-P<sub>GPD</sub>/RAD30-HAP<sub>TEF</sub>/LSM12-Myc</i>	This study
BY4741 UBP3-HA LSM12-Myc mutant	<i>Mata his3Δ1 leu2Δ0 met15Δ0 ura3Δ0 UBP3::LEU2 LSM12::HIS3; pY26-P<sub>GPD</sub>/UBP3-HAP<sub>TEF</sub>/LSM12-Myc</i>	This study
BY4741 RAD30-eGFP LSM12-mCherry mutant	<i>Mata his3Δ1 leu2Δ0 met15Δ0 ura3Δ0 RAD30::RAD30-eGFP LSM12::LSM12-mCherry</i>	This study
<b>Plasmids</b>		
pY26	2- $\mu$ m tail length, Amp, URA3, P <sub>GPD</sub> , P <sub>TEF</sub>	Turbo
pGBKT7	Kan <sup>r</sup> , TRP1, GAL4 DNA-binding domain fusion	Clontech
pGADT7	Amp <sup>r</sup> , LEU2, GAL4 DNA-binding domain fusion	Clontech

The plasmids were then transformed into the corresponding deletion mutants, and site-specific mutations were performed by a PCR-based method using the mutagenic primers. All primers used in this study are listed in Tables 3 and 4.

Yeast cells were cultivated in yeast extract peptone dextrose (YPD) medium (1% yeast extract, 2% tryptone, 2% glucose [pH 6.5]) and yeast nitrogen base (YNB) medium (0.67% yeast nitrogen base without amino acids, 2% glucose, and supplemented with adenine [20.25 mg/liter], arginine [20 mg/liter], histidine [20 mg/liter], leucine [60 mg/liter], lysine [200 mg/liter], methionine [20 mg/liter], threonine [300 mg/liter], tryptophan [20 mg/liter], and uracil [20 mg/liter] [pH 6.5]). Yeast cells were grown at 30°C with constant shaking at 200 rpm in a shaker-incubator chamber.

**Spot assays.** Yeast cells were cultivated in the logarithmic phase and diluted to an absorbance of 1.0 at 600 nm ( $A_{600}$ ) in phosphate-buffered saline (pH 7.0). Then, 10-fold serial dilution cells were spotted onto YNB plates containing no drug or the indicated concentrations of H<sub>2</sub>O<sub>2</sub>. For the plates containing H<sub>2</sub>O<sub>2</sub>, the H<sub>2</sub>O<sub>2</sub> was added when the medium temperature was lowered to 40°C, and the plates were used on the same day. Growth was assessed after incubation for 2 to 4 days at 30°C.

**Survival assays.** Yeast cells were cultivated in the logarithmic phase, harvested by centrifugation, washed with sterile water, and resuspended in phosphate-buffered saline (pH 7.0) to obtain 10<sup>4</sup> cells/ml at an optical density of 600 nm (OD<sub>600</sub>). Cells were then treated with various doses of H<sub>2</sub>O<sub>2</sub> for 1 h at 30°C with 200 rpm shaking, followed by centrifugation and washing with sterile water for three times. After dilution, cells were plated on YNB medium plates and incubated at 30°C for 2 to 4 days. Then, the survival colonies were counted. The cell survival of each strain was expressed relative to that of untreated cells of the corresponding strain.

**Single-cell gel electrophoresis.** Single-cell gel electrophoresis was performed according to the protocol adopted for yeast cells (48). Approximately 10<sup>6</sup> cells were harvested by centrifugation (2 min at 18,000  $\times$  g, 4°C) and mixed with 1.5% (wt/vol) low-melting agarose in S buffer (1 M sorbitol, 25 mM KH<sub>2</sub>PO<sub>4</sub> [pH 6.5]) containing approximately 2 mg/ml Zymolyase (20T; 20,000 U/g); 80  $\mu$ l of this mixture was spread over a slide coated with a water solution of 0.5% (wt/vol) normal-melting

**TABLE 3** Primers used for plasmid construction in this study

Primer by function	Sequence (5'–3') <sup>a</sup>
Deletion	
L-RAD30-F1	G TTCAGGCTCTGCAACTGG
L-RAD30-F2	G ATCTTCTTAGGGGCGACATGCTTTGTCTTGTTTATCAAAGC
LEU2(RAD30)-F1	G CTTTGATAAAAACAAGACAAAGCATGTCTGCCCTAAGAAGATC
LEU2(RAD30)-F2	C CATATAATTGTCTATTTGGAAATAGGTTAAGCAAGGATTTCTTAACCTC
R-RAD30-F1	G AAGTTAAGAAAATCCTTGCTTAACCTATTCCAAATAGACAATTATATGG
R-RAD30-F2	G GTCTTCAGAAAGATGATGATAGTG
L-VHR2-F1	C CACCTGTTCGGCAATTTTTG
L-VHR2-F2	A GGGCTTTCTGCTCTGCATCTTGCAATTTTTACTCTGAC
HIS3(VHR2)-F1	G TCAGAGTAAAAATTGCAAGATGACAGAGCAGAAAGCCCT
HIS3(VHR2)-F2	G GGGGATGATGCAAGCGGGCCTATCTACATAAGAACACCTTTGG
R-VHR2-F1	C CAAAGGTGTTCTTATGTAGATAGGCCGCTTGCATCATCCCC
R-VHR2-F2	C TGAAGAACTGGGCCTTGTCT
L-BAP3-F1	G GCACCTTCTCGTTTCTTCATC
L-BAP3-F2	G GGGCTTTCTGCTCTGTCATTACCTTAGGGGAAAGAAAATATTA
HIS3(BAP3)-F1	T AATATTTTCTTTCCCTAAGGTAATGACAGAGCAGAAAGCCC
HIS3(BAP3)-F2	T AAAATGCTATTTATTATGCACTACATAAGAACACCTTTGGTG
R-BAP3-F1	C CACCAAAGGTGTTCTTATGTAGTGCATAAATAAGCATTTT
R-BAP3-F2	G TATATACACCACTATCGCCAC
L-PHO3-F1	G CAGCGTCAGTAACTCTACTG
L-PHO3-F2	C TAGGGCTTTCTGCTCTGCATAGGTAATTTGGAATGGCCC
HIS3(PHO3)-F1	G GGGCCATCCAAATTACCTATGACAGAGCAGAAAGCCCTAG
HIS3(PHO3)-F2	A ATATTTATTTATATACAATCTACATAAGAACACCTTTGGTG
R-PHO3-F1	C CACCAAAGGTGTTCTTATGTAGATTGTATAAATAAATAATAT
R-PHO3-F2	C CATCAGCTATTTCTTTGGCCAC
L-LSM12-F1	C CATAAGTTGAAGCCGGGCA
L-LSM12-F2	C TAGGGCTTTCTGCTCTGTCATGGACGAAAGATGCAATTG
HIS3(LSM12)-F1	C AATTTGCACTTTCTGCTCCATGACAGAGCAGAAAGCCCTAG
HIS3(LSM12)-F2	A TCCGTTCCGTCATTAATTAATCTACATAAGAACACCTTTGG
R-LSM12-F1	C ACCAAAGGTGTTCTTATGTAGATTAATTAATGACGGAAACGAT
R-LSM12-F2	C ATCGGAAGTCAGTTCTGGTG
L-YHB1-F1	G GACCGCTTATGCGTCTTC
L-YHB1-F2	T AGGGCTTTCTGCTCTGCATAATGAATAAAGTCTTTGTGT
HIS3(YHB1)-F1	A CACAAAGACTTTATTCATTATGACAGAGCAGAAAGCCCTA
HIS3(YHB1)-F2	G GAAGTTTCCGAGGCTTAACGCCTACATAAGAACACCTTTGGT
R-YHB1-F1	C CACCAAAGGTGTTCTTATGTAGGCGTTAAGCCTCGGAAACTTC
R-YHB1-F2	C ATGCCATTATACTGGGGTC
L-PTR2-F1	C CCGCCCTACTGACATCCTG
L-PTR2-F2	A GGGCTTTCTGCTCTGCATTATAAGAGTTTATTAGTGAT
HIS3(PTR2)-F1	G GATCATAATAAACTCTTATAATGACAGAGCAGAAAGCCC
HIS3(PTR2)-F2	G GACAGTAAAGTTAATTAACGCACTACATAAGAACACCTTTGGT
R-PTR2-F1	C ACCAAAGGTGTTCTTATGTAGTGCCTTAATTAACCTACTGTC
R-PTR2-F2	C CACACCAACCAATTGCGTCC
L-CAR1-F1	C CACATCATACGGATGAACTACG
L-CAR1-F2	C TAGGGCTTTCTGCTCTGTCATCTTGATAGTAGTTATTGTTAT
HIS3(CAR1)-F1	A ATAACAATAACTACTATCAAGATGACAGAGCAGAAAGCCCTAG
HIS3(CAR1)-F2	G GATAAAAGGGATGATGATATAAACTACATAAGAACACCTTTGG
R-CAR1-F1	C ACCAAAGGTGTTCTTATGTAGTTTATATCATCATCCCTTTTATC
R-CAR1-F2	G AGGTGGAAGTGAACAGATGGC
L-NDE1-F1	G ATGCTCGAGATGCCCTG
L-NDE1-F2	C TAGGGCTTTCTGCTCTGCATTATTATTGGTTAATTTTTTAT
HIS3(NDE1)-F1	A AATAAAAAATTAACCAATAATAATGACAGAGCAGAAAGCCCTAG
HIS3(NDE1)-F2	T TATTCTCTGTATCTATTTCTACTACATAAGAACACCTTTGG
R-NDE1-F1	G CCAAAGGTGTTCTTATGTAGTAAATAGATACAAGAGAATAA
R-NDE1-F2	G GCAATTCAGGATTCACATGGG
L-UBP2-F1	C CCGCTCAAGCATGATTCGT
L-UBP2-F2	C TAGGGCTTTCTGCTCTGTCATTTCCCTATACCTTCTTAACC
HIS3(UBP2)-F1	G GGTAAAGAAGGTATAAGGAAATGACAGAGCAGAAAGCCCTAG
HIS3(UBP2)-F2	A TAAACTCTTATTGACTAAGACTACATAAGAACACCTTTGGT
R-UBP2-F1	C ACCAAAGGTGTTCTTATGTAGTCTTACTAGTCAATGAAGAGTTTAT
R-UBP2-F2	T TGATATTCTCTCCCTCGTCGTC
L-UBP3-F1	G GCGGCTATTTACTTGGATCAC
L-UBP3-F2	T TAGGGCTTTCTGCTCTGTCATTTTTTTAATGATGATGGAA
HIS3(UBP3)-F1	T TCCATCATCATTAAAAAAATGACAGAGCAGAAAGCCCTA
HIS3(UBP3)-F2	G TCTATAATACCACCCCCGCTCTACATAAGAACACCTTTGG
R-UBP3-F1	C CCAAAGGTGTTCTTATGTAGGACGGGGGTGGTATTATAGAC

(Continued on next page)

**TABLE 3** (Continued)

Primer by function	Sequence (5'–3') <sup>a</sup>
R-UBP3-F2	GTGTTGGACTCATCGTCTGTG
L-UBP15-F1	CGAGTGTGAAAAAAGTCGCTAC
L-UBP15-F2	<u>CTAGGGCTTTCTGCTCTGTCATTGTTTGTGTTGAAGAGACTAAT</u>
HIS3(UBP15)-F1	<u>GATTAGTCTCTTCAAACAACAATGACAGAGCAGAAAAGCCCTA</u>
HIS3(UBP15)-F2	<u>CTAAACATAGTCGTAAGACGCTACATAAAGAACACCTTTGGT</u>
R-UBP15-F1	<u>ACCAAAGGTGTTCTTATGTAGTACGCTTACGACTATGTTAG</u>
R-UBP15-F2	<u>TAAAGCAAACCAAGAAGCCG</u>
<b>Overexpression</b>	
RAD30-F1	<u>CCCAAGCTTATGTCAAATTTACTTGGAAGGAG</u>
RAD30-F2	<u>CCGCTCGAGTCATTTTTTCTGTAAAAAATGAT</u>
VHR-F1	<u>CCCAAGCTTATGAGCTCTGAAGACGAATTGG</u>
VHR-F2	<u>CCGCTCGAGTCAGTTTTAATGATCATTGGTC</u>
BAP3-F1	<u>CCCAAGCTTATGTCAGATCCTATAGTAACGTC</u>
BAP3-F2	<u>CCGCTCGAGCTAACACCAAATTTGTAGACTCT</u>
PHO3-F1	<u>CCCAAGCTTATGTTAAGTCTGTTGTTTATTCGG</u>
PHO3-F2	<u>CCGCTCGAGTTATTGTTTTAATAGGGTATCGTTG</u>
LSM12-F1	<u>CCGGAATTCATGAGTGTACGCTTGAGCAA</u>
LSM12-F2	<u>CCGCTCGAGCTATCCACCTTCTACCATC</u>
YHB1-F1	<u>CCCAAGCTTATGCTAGCGAAAAAACCCG</u>
YHB1-F2	<u>CCGCTCGAGCTAACTTGCACGGTTGACAT</u>
PTR2-F1	<u>CCCAAGCTTATGCTCAACCATCCAGCC</u>
PTR2-F2	<u>CCGCTCGAGCTAATATTGGTGGTGGATCTTAG</u>
CAR1-F1	<u>CCGGAATTCATGGAACAGGACCTCATTACAA</u>
CAR1-F2	<u>CCGCTCGAGCTACAATAAGGTTTACCCAATGC</u>
NDE1-F1	<u>CCGGAATTCATGATTAGACAATCATTAAATGAAAA</u>
NDE1-F2	<u>CCGCTCGAGCTAGATAGATGAATCTCTACCCAAG</u>
<b>Point mutation</b>	
RAD30/D570A-F1	AGAGCACGCAGCCTATCATTAGCA
RAD30/D570A-F2	TGCTAAATGATAGGCTGCGTGCTCT
RAD30/F627,628AA-F1	CCAAAAACATCTTATCAGCCGCTACAAGAAAAAATGA
RAD30/F627,628AA-F2	TCATTTTTTCTTGTAGCGGCTGATAAGATGTTTTTGG
<b>Yeast two-hybrid assay</b>	
BD-RAD30-F1	ACGCGTCGACATGTCAAAATTTACTTGGAAGGAG
BD-RAD30-F2	TGCACTGCAGTCATTTTTTCTGTAAAAAATGA
BD-UBP3-F1	CCGGAATTCATGAACATGCAAGACGCTAAC
BD-UBP3-F2	TGCAGTGCAGTTAATTTCTTTTTGATACATTA
AD-LSM12-F1	CCGGAATTCATGAGTGTACGCTTGAGC
AD-LSM12-F2	CCGCTCGAGCTATCCACCTTCTACCATCG
<b>Coimmunoprecipitation</b>	
pY26/P <sub>GPD</sub> -RAD30-F1	CCGGAATTCATGTCAAATTTACTTGGAAGGAG
pY26/P <sub>GPD</sub> -RAD30-F2	GGCGAGCTCTTAAGCGTAGTCTGGGACGTCGTATGGGTATTTTTTCTGTAAAAAATGAT
pY26/P <sub>TEF</sub> -LSM12-F1	TAAAGCGGCCGATGAGTGTACGCTTGAGCAAAC
pY26/P <sub>TEF</sub> -LSM12-F2	GGAAGATCTTTACAGATCCTTTCAGAGATGAGTTTCTGCTCTCCACCTTCTACCATCGTC
pY26/P <sub>GPD</sub> -UBP3-F1	<u>CCCAAGCTTATGAACATGCAAGACGCTAACAA</u>
pY26/P <sub>GPD</sub> -UBP3-F2	<u>CCGCTCGAGTTAAGCGTAGTCTGGGACGTCGTATGGTAATTTCTTTTTGATACATTAATA</u>
<b>Subcellular localization</b>	
RAD30-F1	<u>CCGGAATTCATGTCAAATTTACTTGGAAGGAG</u>
RAD30-F2	<u>TCGCCCTTGCTCACCATGCCGCTCCTCTTTTTTCTGTAAAAAATG</u>
eGFP-F1	<u>ATTTTTTACAAGAAAAAAGGAGGAGGCGGATGGTGAGCAAGGGCGAGGAG</u>
eGFP-F2	<u>CCGCTCGAGTTACTTGTACAGCTCGTCCATG</u>
LSM12-F1	<u>TAAAGCGGCCGATGAGTGTACGCTTGAGCAAAC</u>
LSM12-F2	<u>TCCTCGCCCTTGCTCACCATGCCGCTCCTCCTCCACCTTCTACCATCGT</u>
mCherry-F1	<u>GACGATGGTAGGAAAGGTGGAGGAGGAGGCGGATGGTGAGCAAGGGCGAGG</u>
mCherry-F2	<u>GGAAGATCTTTACTTGTACAGCTCGTCCATG</u>

<sup>a</sup>Underlining represents sequences of regions flanking a target gene or a restriction site.

agarose, covered with a coverslip, and incubated for 30 min at 30°C for cell wall enzymatic degradation, after which the coverslips were removed. All further procedures were performed in a cold room at 4°C. Slides were incubated in a lysis buffer (30 mM NaOH, 1 M NaCl, 0.05% lauryl sarcosine, 50 mM EDTA, 10 mM Tris-HCl [pH 10]) for 2 h to lyse yeast spheroplasts. The slides were washed three times for 20 min each in electrophoresis buffer (30 mM NaOH, 10 mM EDTA, 10 mM

**TABLE 4** Primers used for RT-PCR in this study

Primer	Sequence (5'–3')
VHR2-F	GGAGATGTCTAAGGATGA
VHR2-R	AGCCGTTCAGTAAGATAT
BAP3-F	GCTCCAGGTAACCTCAA
BAP3-R	GTAATCAATCCAACGGTAG
PHO3-F	CGGCTCATTGTCTTCT
PHO3-R	ATCCATCTCACCAGTGTAT
LSM12-F	CCAACAACACTCTTACTATCCAA
LSM12-R	GCTTATACCAATGACTTCCA
YHB1-F	GCTAAGAACATTGACGATT
YHB1-R	TTGGATAATGCTCAGGTT
PTR2-F	TTGTTCTGGTTGTCTTCA
PTR2-R	ATTCGTCTTCTTCTCGTAGTC
CAR1-F	GAAACAAACGGTGAAGGT
CAR1-R	TGTAGCAGGAATGTATAATGG
NDE1-F	GTGCTCTGGCTTATATTG
NDE1-R	AGAATAGGAAGGTGAATGA
RAD30-F	CGAGTATTGATGAAGTATT
RAD30-R	GGTATAAGAGGTAGATGG

Tris-HCl [pH 10]) to remove the lysis solution. The slides were then submitted to electrophoresis in the same buffer for 15 min at 0.7 V/cm. After electrophoresis, the slides were incubated in a neutralization buffer (10 mM Tris-HCl [pH 7.4]) for 10 min, followed by consecutive 5-min incubations in 76% and 96% ethanol. The slides were then air-dried and visualized immediately or stored at 4°C for later observation. For visualization in the fluorescence microscope, the slides were stained with ethidium bromide (10  $\mu$ g/ml), and 20 representative images of each slide were acquired at a magnification of  $\times$ 400 using a Leica Microsystems DM fluorescence microscope. The images were analyzed with the help of the free edition of Comet Assay Software Project (CASP), and the analytic parameter tail length (in micrometers) was chosen as the unit of DNA damage. In each slide, at least 20 comets were analyzed, and error bars in the figures represent variability between the mean of at least three different slides obtained from biologically independent experiments.

**Genome-wide transcription analysis.** The wild-type and *rad30* $\Delta$  mutant strains were cultivated in the logarithmic phase, and H<sub>2</sub>O<sub>2</sub> was added to obtain a final concentration of 2 mM; cells were collected after 1 h of H<sub>2</sub>O<sub>2</sub> treatment. Total RNA was isolated using MiniBEST universal RNA extraction kit (TaKaRa Bio, Shiga, Japan). The concentration and quality of total RNA were determined by microspectrophotometry using an Agilent 2100 Bioanalyzer (Agilent Technologies, Santa Clara, CA). Frozen samples were sent to the Majorbio Institute for global gene analysis.

**Quantitative reverse transcription-PCR analysis.** Cells were cultivated in the logarithmic phase and then treated with 2 mM H<sub>2</sub>O<sub>2</sub> for 1 h. Total RNA was extracted using the MiniBEST universal RNA extraction kit (TaKaRa Bio, Shiga, Japan), and cDNA was synthesized using the PrimeScript II 1st-strand cDNA synthesis kit (catalog no. 6210A; TaKaRa Bio). Quantitation of mRNA level was performed using SYBR Premix *Ex Taq* (catalog no. RR420A; TaKaRa Bio). *ACT1* was used as a standard control to normalize the gene expression.

**Yeast two-hybrid assays.** All Y2H plasmids were based on either pGBKT7 (Gal<sub>4</sub><sub>BD</sub>) or pGADT7 (Gal<sub>4</sub><sub>AD</sub>). pGBKT7-*RAD30*, pGADT7-*LSM12*, pGADT7-*UBP3*, and other point mutant fusion protein plasmids were constructed by standard genetic techniques. In order to be tested, the Gal<sub>4</sub><sub>AD</sub> and Gal<sub>4</sub><sub>BD</sub> plasmids were cotransformed into the yeast *AH109* mutant strain. Individual colonies were then picked and allowed to grow at 30°C on a synthetic defined (SD)-Leu-Trp plate for 2 to 3 days, after which transformants were printed on SD-Leu-Trp, SD-Leu-Trp-Ade, and SD-Leu-Trp-His selective plates with or without a certain amount of the histidine biosynthesis inhibitor 1,2,4-aminotriazole (3-AT) (49).

**Western blotting.** Pol $\eta$  and PCNA containing a C-terminal hemagglutinin (HA) tag were expressed from their native promoters in the wild-type and *lsm12* $\Delta$  mutant strains. Cells were grown to logarithmic phase, harvested by centrifugation, and then resuspended in lysis buffer containing 50 mM Tris-HCl (pH 7.5), 150 mM NaCl, 1 mM EDTA, 10% (vol/vol) glycerol, 0.1% Tween 20, 1 mM phenylmethylsulfonyl fluoride (PMSF), and 1 $\times$  complete protease inhibitor mixture (Sangon Biotech). Cells were broken by bead beating (45 min at 4°C) with glass beads, and the supernatant was collected. The extracts were resolved by SDS-PAGE in 10% acrylamide gels, transferred to a polyvinylidene difluoride (PVDF) membrane, and blocked with 5% milk in Tris-buffered saline with Tween 20 (TBST). The monoubiquitination levels of Pol $\eta$  and PCNA were probed with mouse anti-HA tag antibody (ab18181) and rabbit anti-mouse IgG secondary antibodies conjugated to horseradish peroxidase (HRP; ab6728). The bands were visualized using a ChemiDoc XRS+ imaging system.

**Coimmunoprecipitation.** Cells were transformed with indicated plasmids, and total proteins were extracted by lysis buffer. The extracts were incubated with 25  $\mu$ l anti-HA-conjugated magnetic beads (Bio-Rad) overnight at 4°C and washed three times with lysis buffer. Next, the precipitates were eluted into 100 mM glycine (pH 2.5) and 100 mM NaCl and immediately neutralized with 2 M Tris-HCl (pH 9.0) and 100 mM NaCl, and then the immunoblot analysis was performed.

**Microscopic analysis.** Microscopic analysis was performed as previously described (50, 51), with slight modifications. Yeast strains were cultivated in logarithmic phase and then incubated with 2 mM

H<sub>2</sub>O<sub>2</sub> for 2 h or 0.12% MMS for 1 h. The cells were then harvested by centrifugation and washed with 0.1 M phosphate buffer (PBS; pH 7.5). The pellet was resuspended in 20  $\mu$ l of 0.1 M PBS with 1.2 M sorbitol for microscopy. Images were obtained with Leica TCS SP8 confocal microscope using 488 nm for enhanced green fluorescent protein (eGFP). The percentage of cells with foci was calculated from three independent experiments and at least 500 cells per experiment.

**Quantification and statistical analysis.** For quantification of the Western blot data, the ImageJ software was used to measure the relative intensity of each band, and the relative PCNA-Ub and Pol $\eta$ -Ub protein levels were normalized to the relative  $\beta$ -actin levels. Quantification data are presented as the mean  $\pm$  standard deviation from at least three independent experiments. Statistical differences were determined by the *t* test.

**Data availability.** The raw data are available at [SRP151558](https://doi.org/10.1101/151558), and detailed descriptions are included in the supplemental material. The annotation and the Gene Ontology (GO) were based on the *Saccharomyces* Genome Database (SGD).

## SUPPLEMENTAL MATERIAL

Supplemental material for this article may be found at <https://doi.org/10.1128/AEM.01988-18>.

**SUPPLEMENTAL FILE 1**, PDF file, 0.4 MB.

**SUPPLEMENTAL FILE 2**, XLS file, 0.8 MB.

**SUPPLEMENTAL FILE 3**, XLS file, 3.2 MB.

**SUPPLEMENTAL FILE 4**, XLS file, 3.2 MB.

## ACKNOWLEDGMENTS

This work was supported by the National Natural Science Foundation of China (grants 21576117 and 21878126), the Key Technologies R & D Program of Jiangsu Province (grant BE2015307), the National First-Class Discipline Program of Light Industry Technology and Engineering (grant LITE2018-20), and the Top-Notch Academic Programs Project of Jiangsu Higher Education Institution (grant PPZY2015B146).

R.Y., L.L., and J.W. designed the research; R.Y., L.S., C.W., and W.Q. performed the research; R.Y. and J.W. analyzed the data; and R.Y. and L.L. wrote the paper.

We declare no competing financial interests.

## REFERENCES

1. Novarina D, Mavrova SN, Janssens GE, Rempel IL, Veenhoff LM, Chang M. 2017. Increased genome instability is not accompanied by sensitivity to DNA damaging agents in aged yeast cells. *DNA Repair (Amst)* 54:1–7. <https://doi.org/10.1016/j.dnarep.2017.03.005>.
2. Hayashi MT, Cesare AJ, Rivera T, Karlseder J. 2015. Cell death during crisis is mediated by mitotic telomere deprotection. *Nature* 522:492–496. <https://doi.org/10.1038/nature14513>.
3. Saini P, Beniwal A, Vij S. 2017. Physiological response of *Kluyveromyces marxianus* during oxidative and osmotic stress. *Process Biochem* 56: 21–29. <https://doi.org/10.1016/j.procbio.2017.03.001>.
4. Zhao HW, Li JY, Han BZ, Li X, Chen JY. 2014. Improvement of oxidative stress tolerance in *Saccharomyces cerevisiae* through global transcription machinery engineering. *J Ind Microbiol Biotechnol* 41:869–878. <https://doi.org/10.1007/s10295-014-1421-8>.
5. Roukas T. 2016. The role of oxidative stress on carotene production by *Blakeslea trispora* in submerged fermentation. *Crit Rev Biotechnol* 36: 424–433.
6. Naiman K, Pages V, Fuchs RP. 2016. A defect in homologous recombination leads to increased translesion synthesis in *E. coli*. *Nucleic Acids Res* 44:7691–7699. <https://doi.org/10.1093/nar/gkw488>.
7. Fumasoni M, Zwicky K, Vanoli F, Lopes M, Branzei D. 2015. Error-free DNA damage tolerance and sister chromatid proximity during DNA replication rely on the Pol $\alpha$ /primase/Ctf4 complex. *Mol Cell* 57:812–823. <https://doi.org/10.1016/j.molcel.2014.12.038>.
8. Villoria MT, Ramos F, Duenas E, Faull P, Cutillas PR, Clemente-Blanco A. 2017. Stabilization of the metaphase spindle by Cdc14 is required for recombinational DNA repair. *EMBO J* 36:79–101. <https://doi.org/10.15252/emboj.201593540>.
9. Shemesh K, Sebesta M, Pacesa M, Sau S, Bronstein A, Parnas O, Liefshitz B, Venclovas C, Krejci L, Kupiec M. 2017. A structure-function analysis of the yeast Elg1 protein reveals the importance of PCNA unloading in genome stability maintenance. *Nucleic Acids Res* 45:3189–3203. <https://doi.org/10.1093/nar/gkw1348>.
10. Gervai JZ, Galiczka J, Szeltner Z, Zamborszky J, Szuts D. 2017. A genetic study based on PCNA-ubiquitin fusions reveals no requirement for PCNA polyubiquitylation in DNA damage tolerance. *DNA Repair (Amst)* 54: 46–54. <https://doi.org/10.1016/j.dnarep.2017.04.003>.
11. Northam MR, Trujillo KM. 2016. Histone H2B mono-ubiquitylation maintains genomic integrity at stalled replication forks. *Nucleic Acids Res* 44:9245–9255. <https://doi.org/10.1093/nar/gkw658>.
12. Zhang SC, Wang LL, Tao Y, Bai TY, Lu R, Zhang TL, Chen JY, Ding JP. 2017. Structural basis for the functional role of the Shu complex in homologous recombination. *Nucleic Acids Res* 45:13068–13079. <https://doi.org/10.1093/nar/gkx992>.
13. Budzowska M, Graham TGW, Soback A, Waga S, Walter JC. 2015. Regulation of the Rev1-pol zeta complex during bypass of a DNA interstrand cross-link. *EMBO J* 34:1971–1985. <https://doi.org/10.15252/emboj.201490878>.
14. Rechkooblit O, Kolbanovskiy A, Landes H, Geacintov NE, Aggarwal AK. 2017. Mechanism of error-free replication across benzo[a]pyrene stereoisomers by Rev1 DNA polymerase. *Nat Commun* 8:965. <https://doi.org/10.1038/s41467-017-01013-5>.
15. Huang M, Zhou B, Gong J, Xing L, Ma X, Wang F, Wu W, Shen H, Sun C, Zhu X, Yang Y, Sun Y, Liu Y, Tang T-S, Guo C. 2018. RNA-splicing factor SART3 regulates translesion DNA synthesis. *Nucleic Acids Res* 46: 4560–4574. <https://doi.org/10.1093/nar/gky220>.
16. Yang Y, Gao Y, Mutter-Rottmayer L, Zlatanou A, Durando M, Ding W, Wyatt D, Ramsden D, Tanoue Y, Tateishi S, Vaziri C. 2017. DNA repair factor RAD18 and DNA polymerase Pol $\kappa$  confer tolerance of oncogenic DNA replication stress. *J Cell Biol* 216:3097–3115. <https://doi.org/10.1083/jcb.201702006>.
17. Vujanovic M, Krietsch J, Raso MC, Terraneo N, Zellweger R, Schmid JA, Tagliatalata A, Huang J-W, Holland CL, Zwicky K, Herrador R, Jacobs H, Cortez D, Ciccia A, Penengo L, Lopes M. 2017. Replication fork slowing and reversal upon DNA damage require PCNA polyubiquitylation and

- ZRANB3 DNA translocase activity. *Mol Cell* 67:882–890. <https://doi.org/10.1016/j.molcel.2017.08.010>.
18. Vaisman A, Woodgate R. 2017. Translesion DNA polymerases in eukaryotes: what makes them tick? *Crit Rev Biochem Mol Biol* 52:274–303. <https://doi.org/10.1080/10409238.2017.1291576>.
  19. Tellier-Lebegue C, Dizet E, Ma E, Veaute X, Coic E, Charbonnier JB, Maloisel L. 2017. The translesion DNA polymerases Pol  $\zeta$  and Rev1 are activated independently of PCNA ubiquitination upon UV radiation in mutants of DNA polymerase delta. *PLoS Genet* 13:e1007119. <https://doi.org/10.1371/journal.pgen.1007119>.
  20. Sale JE, Lehmann AR, Woodgate R. 2012. Y-family DNA polymerases and their role in tolerance of cellular DNA damage. *Nat Rev Mol Cell Biol* 13:141–152. <https://doi.org/10.1038/nrm3289>.
  21. De Palma A, Morren MA, Ged C, Pouvelle C, Taieb A, Aoufouchi S, Sarasin A. 2017. Diagnosis of xeroderma pigmentosum variant in a young patient with two novel mutations in the POLH gene. *Am J Med Genet* 173:2511–2516. <https://doi.org/10.1002/ajmg.a.38340>.
  22. Xue QZ, Zhong MY, Liu BY, Tang Y, Wei ZL, Guengerich FP, Zhang HD. 2016. Kinetic analysis of bypass of 7,8-dihydro-8-oxo-2'-deoxyguanosine by the catalytic core of yeast DNA polymerase  $\eta$ . *Biochimie* 121:161–169. <https://doi.org/10.1016/j.biochi.2015.12.009>.
  23. Choi JH, Pfeifer GP. 2005. The role of DNA polymerase  $\eta$  in UV mutational spectra. *DNA Repair (Amst)* 4:211–220. <https://doi.org/10.1016/j.dnarep.2004.09.006>.
  24. Liu BY, Xue QZ, Gu SL, Wang WP, Chen J, Li YQ, Wang CX, Zhang HD. 2016. Kinetic analysis of bypass of O<sup>6</sup>-methylguanine by the catalytic core of yeast DNA polymerase  $\eta$ . *Arch Biochem Biophys* 596:99–107. <https://doi.org/10.1016/j.abb.2016.03.009>.
  25. Yang JT, Wang R, Liu BY, Xue QZ, Zhong MY, Zeng H, Zhang HD. 2015. Kinetic analysis of bypass of abasic site by the catalytic core of yeast DNA polymerase  $\eta$ . *Mutat Res* 779:134–143. <https://doi.org/10.1016/j.mrfmmm.2015.07.001>.
  26. Saito Y, Zhou H, Kobayashi J. 2015. Chromatin modification and NBS1: their relationship in DNA double-strand break repair. *Genes Genet Syst* 90:195–208. <https://doi.org/10.1266/ggs.15-00010>.
  27. Boehm EM, Powers KT, Kondratick CM, Spies M, Houtman JCD, Washington MT. 2016. The proliferating cell nuclear antigen (PCNA)-interacting protein (PIP) motif of DNA polymerase  $\eta$  mediates its interaction with the C-terminal domain of Rev1. *J Biol Chem* 291:8735–8744. <https://doi.org/10.1074/jbc.M115.697938>.
  28. Boehm EM, Spies M, Washington MT. 2016. PCNA tool belts and polymerase bridges form during translesion synthesis. *Nucleic Acids Res* 44:8250–8260. <https://doi.org/10.1093/nar/gkw563>.
  29. Ai YX, Wang JL, Johnson RE, Haracska L, Prakash L, Zhuang ZH. 2011. A novel ubiquitin binding mode in the *S. cerevisiae* translesion synthesis DNA polymerase  $\eta$ . *Mol Biosyst* 7:1874–1882. <https://doi.org/10.1039/c0mb00355g>.
  30. Donigan KA, Cerritelli SM, McDonald JP, Vaisman A, Crouch RJ, Woodgate R. 2015. Unlocking the steric gate of DNA polymerase  $\eta$  leads to increased genomic instability in *Saccharomyces cerevisiae*. *DNA Repair (Amst)* 35:1–12. <https://doi.org/10.1016/j.dnarep.2015.07.002>.
  31. Wit N, Buoninfante OA, van den Berk PCM, Jansen JG, Hogenbirk MA, de Wind N, Jacobs H. 2015. Roles of PCNA ubiquitination and TLS polymerases  $\kappa$  and  $\eta$  in the bypass of methyl methanesulfonate-induced DNA damage. *Nucleic Acids Res* 43:282–294. <https://doi.org/10.1093/nar/gku1301>.
  32. Chen X, Bosques L, Sung P, Kupfer GM. 2016. A novel role for non-ubiquitinated FANCD2 in response to hydroxyurea-induced DNA damage. *Oncogene* 35:22–34. <https://doi.org/10.1038/ncr.2015.68>.
  33. de Moura MB, Fonseca Schamber-Reis BL, Passos Silva DG, Rajao MA, Macedo AM, Franco GR, Junho Pena SD, Ribeiro Teixeira SM, Machado CR. 2009. Cloning and characterization of DNA polymerase  $\eta$  from *Trypanosoma cruzi*: roles for translesion bypass of oxidative damage. *Environ Mol Mutagen* 50:375–386. <https://doi.org/10.1002/em.20450>.
  34. Zlatanou A, Despras E, Braz-Petta T, Boubakour-Azzouz I, Pouvelle C, Stewart GS, Nakajima S, Yasui A, Ishchenko AA, Kannouche PL. 2011. The hMsh2-hMsh6 complex acts in concert with monoubiquitinated PCNA and Pol  $\eta$  in response to oxidative DNA damage in human cells. *Mol Cell* 43:649–662. <https://doi.org/10.1016/j.molcel.2011.06.023>.
  35. Fleischer TC, Weaver CM, McAfee KJ, Jennings JL, Link AJ. 2006. Systematic identification and functional screens of uncharacterized proteins associated with eukaryotic ribosomal complexes. *Genes Dev* 20:1294–1307. <https://doi.org/10.1101/gad.1422006>.
  36. Lee MW, Kim BJ, Choi HK, Ryu MJ, Kim SB, Kang KM, Cho EJ, Youn HD, Huh WK, Kim ST. 2007. Global protein expression profiling of budding yeast in response to DNA damage. *Yeast* 24:145–154. <https://doi.org/10.1002/yea.1446>.
  37. Acharya N, Brahma A, Haracska L, Prakash L, Prakash S. 2007. Mutations in the ubiquitin binding UBZ motif of DNA polymerase  $\eta$  do not impair its function in translesion synthesis during replication. *Mol Cell Biol* 27:7266–7272. <https://doi.org/10.1128/MCB.01196-07>.
  38. van der Kemp PA, de Padula M, Burguiere-Slezak G, Ulrich HD, Boiteux S. 2009. PCNA monoubiquitylation and DNA polymerase  $\eta$  ubiquitin-binding domain are required to prevent 8-oxoguanine-induced mutagenesis in *Saccharomyces cerevisiae*. *Nucleic Acids Res* 37:2549–2559. <https://doi.org/10.1093/nar/gkp105>.
  39. Enervald E, Lindgren E, Katou Y, Shirahige K, Strom L. 2013. Importance of Pol  $\eta$  for damage-induced cohesion reveals differential regulation of cohesion establishment at the break site and genome-wide. *PLoS Genet* 9:e1003158. <https://doi.org/10.1371/journal.pgen.1003158>.
  40. Lau WCY, Li YY, Zhang QF, Huen MSY. 2015. Molecular architecture of the Ub-PCNA/pol  $\eta$  complex bound to DNA. *Sci Rep* 5:15759. <https://doi.org/10.1038/srep15759>.
  41. Haracska L, Unk I, Prakash L, Prakash S. 2006. Ubiquitylation of yeast proliferating cell nuclear antigen and its implications for translesion DNA synthesis. *Proc Natl Acad Sci U S A* 103:6477–6482. <https://doi.org/10.1073/pnas.0510924103>.
  42. Pabla R, Rozario D, Siede W. 2008. Regulation of *Saccharomyces cerevisiae* DNA polymerase  $\eta$  transcript and protein. *Radiat Environ Biophys* 47:157–168. <https://doi.org/10.1007/s00411-007-0132-1>.
  43. Bienko M, Green CM, Sabbioneda S, Crosetto N, Matic I, Hibbert RG, Begovic T, Niimi A, Mann M, Lehmann AR, Dikic I. 2010. Regulation of translesion synthesis DNA polymerase  $\eta$  by monoubiquitination. *Mol Cell* 37:396–407. <https://doi.org/10.1016/j.molcel.2009.12.039>.
  44. Álvarez V, Viñas L, Gallego-Sánchez A, Andrés S, Sacristán MP, Bueno A. 2016. Orderly progression through S-phase requires dynamic ubiquitylation and deubiquitylation of PCNA. *Sci Rep* 6:25513. <https://doi.org/10.1038/srep25513>.
  45. Bilsland E, Hult M, Bell SD, Sunnerhagen P, Downs JA. 2007. The Bre5/Ubp3 ubiquitin protease complex from budding yeast contributes to the cellular response to DNA damage. *DNA Repair (Amst)* 6:1471–1484. <https://doi.org/10.1016/j.dnarep.2007.04.010>.
  46. Mao P, Smerdon MJ. 2010. Yeast deubiquitinase Ubp3 interacts with the 26 S proteasome to facilitate Rad4 degradation. *J Biol Chem* 285:37542–37550. <https://doi.org/10.1074/jbc.M110.170175>.
  47. Baudin A, Ozier-Kalogeropoulos O, Denouel A, Lacroute F, Cullin C. 1993. A simple and efficient method for direct gene deletion in *Saccharomyces cerevisiae*. *Nucleic Acids Res* 21:3329–3330. <https://doi.org/10.1093/nar/21.14.3329>.
  48. Azevedo F, Marques F, Fokt H, Oliveira R, Johansson B. 2011. Measuring oxidative DNA damage and DNA repair using the yeast comet assay. *Yeast* 28:55–61. <https://doi.org/10.1002/yea.1820>.
  49. Xu X, Lin A, Zhou C, Blackwell SR, Zhang Y, Wang Z, Feng Q, Guan R, Hanna MD, Chen Z, Xiao W. 2016. Involvement of budding yeast Rad5 in translesion DNA synthesis through physical interaction with Rev1. *Nucleic Acids Res* 44:5231–5245. <https://doi.org/10.1093/nar/gkw183>.
  50. Tkach JM, Yimit A, Lee AY, Riffle M, Costanzo M, Janschob D, Hendry JA, Ou J, Moffat J, Boone C, Davis TN, Nislow C, Brown GW. 2012. Dissecting DNA damage response pathways by analysing protein localization and abundance changes during DNA replication stress. *Nat Cell Biol* 14:966–976. <https://doi.org/10.1038/ncb2549>.
  51. Fan Q, Xu X, Zhao X, Wang Q, Xiao W, Guo Y, Fu YV. 2018. Rad5 coordinates translesion DNA synthesis pathway by recognizing specific DNA structures in *Saccharomyces cerevisiae*. *Curr Genet* 64:889–899. <https://doi.org/10.1007/s00294-018-0807-y>.